NEW DETECTIONS OF HOLLOWS ON MERCURY USING DEEP LEARNING: FIRST GLOBAL ANALYSIS OF HOLLOW DEGRADATION STATES. Ariel N. Deutsch[1,2], Valentin T. Bickel[3], and David T. Blewett[4], [1]NASA Ames Research Center, Moffett Field, CA, USA (ariel.deutsch@nasa.gov), [2]Bay Area Environmental Research Institute, Moffett Field, CA, USA, [3]Center for Space and Habitability – University of Bern, Bern, CH, [4]Johns Hopkins Applied Physics Laboratory, Laurel, MD, USA.

Introduction: Hollows are some of the most interesting features on Mercury. These small, shallow depressions likely formed via volatile loss and appear to be very geologically young, possibly even forming and evolving today [1–6]. To date, three major classes of hollows have been proposed [4,5], showing a range of reflectance and morphologic characteristics (**Fig. 1**). These three classes may be linked to the developmental sequence of hollows, such that young, active hollows have high visible reflectance and distinct morphologies (rounded, irregular outlines and flat, shallow floors), older hollows have muted reflectance signatures, and expired hollows have softened morphologies.

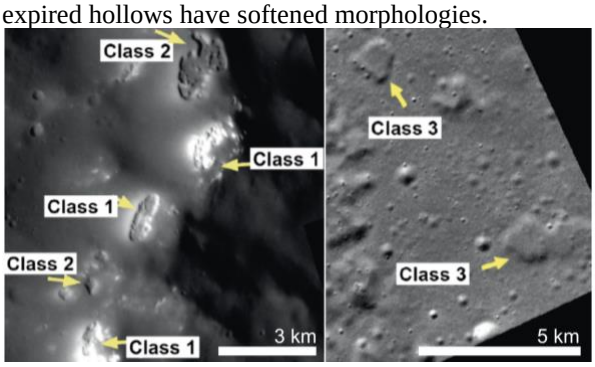

Fig. 1. *Examples of three putative hollow classes [4].*

Important questions remain regarding when, why, and how quickly hollows evolve through these stages. Understanding their distribution and degradation states can help address these questions. We trained a convolutional neural network - the Mercury HOllows Retrieval NETwork (HORNET) - using a Yolov5x instance segmentation architecture (PyTorch 1.7) to automatically detect hollows in MESSENGER Narrow Angle Camera (NAC) images and we are manually classifying their degradation states. Here we report our global results, which include numerous new discoveries of individual hollows and the first global database of hollow degradation states. We are using this database to improve our understanding of hollow evolutionary sequences by analyzing the environments and growth patterns of hollows in various degradation states.

Methods: We employed an iterative human-supervised training and testing approach, outlined here:

HORNET training. To train the HORNET, we generated positive labels (3,016 polygonal outlines of hollows, traced on 162 NAC images) and negative labels (21 NAC images of features that look similar to hollows, including vents, pits, and secondary craters). Positive labels included a diverse set of hollows that vary in number, size, shape, and reflectance properties.

The HORNET received 95% of the training data to learn what is and is not a hollow. During training, image augmentation was used to exponentially grow the training dataset, generating 288,515 total training labels (over 95 training epochs). We developed an augmentation pipeline to represent the full parameter space of NAC images by varying image properties including hue (up to ±80%), saturation (up to ±80%), color value (up to ±80%), rotation (up to ±45°), shear (up to ±10%), scaling (up to ±10%), and X/Y flip (chance of 50%). This augmentation allowed the HORNET to learn what hollows could look like under any MESSENGER imaging conditions. After learning, the HORNET tried to find our human-labelled hollows in the remaining 5% of labels that were unseen during training. It achieved an average precision of 0.63.

HORNET mapping output. We deployed the HORNET on all NAC images with pixel scales ≤120 mpp (N=112,424) using a processing pipeline modified from [7]. The HORNET outputs polygonal shapefiles of hollow candidates identified at three confidence thresholds (CTs): 0.8, 0.7, and 0.6. At higher CTs, precision is higher, but recall (the proportion of actual hollows identified) is lower, as the HORNET tends to miss smaller or more irregular hollows.

Human verification and classification. In less than three minutes, the HORNET output three global candidate databases at CTs 0.8, 0.7, and 0.6. We manually review, verify, and classify every candidate to produce a human-validated dataset of hollows and their classification (**Table 1**).

CT	HORNET Candidates	Verified Detections
0.8	6,887	Complete: 4,755 (69%)
0.7	32,453	So far: 25,257 (78%)
0.6	79,278	Not yet verified

Table 1. *Numbers of HORNET candidates and human-verified detections at different confidence thresholds.*

Preliminary Results: *Hollow degradation states.* The verified global map of hollows from CT=0.8 is shown in **Fig. 2**. The vast majority (~72%) of hollow detections are Class 1. Class 2 hollows make up ~28% of verified detections and only ~0.2% are Class 3. If the classes are indeed linked to hollow evolutionary sequence, then this breakdown suggests most hollows on Mercury can still undergo further development.

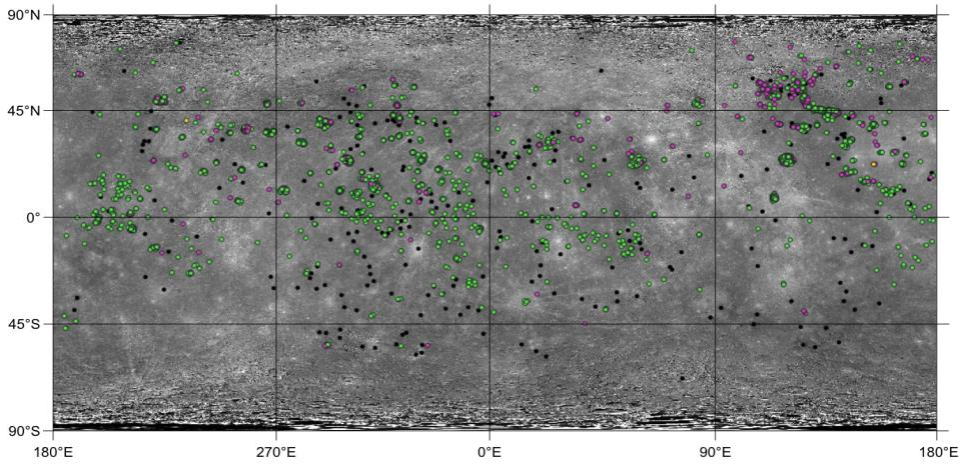

Fig. 2. *Mercury HORNET detections of hollows at CT=0.8, colored by their human-classified degradation state, with Class 1 in green, Class 2 in pink, and Class 3 in yellow. All previously published detections of hollows are in black [1–3]. Basemap is an MDIS low-incidence angle mosaic in an equidistant projection.*

At CT=0.8, HORNET detections are generally consistent with previous human detections of hollows [1–3], but there are still several known detections of hollows that the HORNET missed (**Fig. 2**). Work is ongoing to verify and classify HORNET detections at lower CTs to close these gaps. At lower CTs, we will also see detections of smaller hollows and hollows without high reflectance properties increase.

New detections of hollows. At CT=0.8, the HORNET detections already include many new discoveries (**Fig. 2**). **Fig. 3** illustrates how certain hollows may be easy for humans to miss during mapping endeavors due to small sizes of hollows, muted reflectance properties of hollows, and/or unfavorable illumination geometries of NAC images.

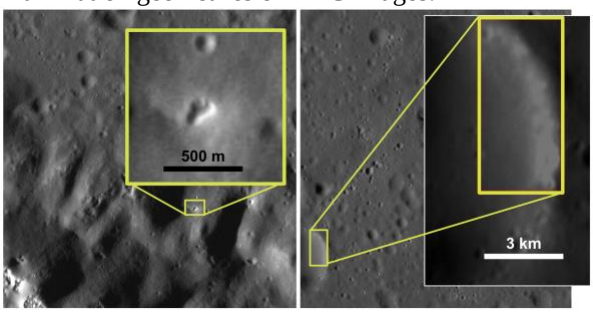

Fig. 3. *Examples of new hollow discoveries. (Left) A small (~150 m) hollow on some mottled impact terrain. (Right) A formation of hollow clusters in a crater rim.*

Local settings of hollows: Here we report initial findings from the verified CT=0.8 data. Classification of hollows at CT=0.7 and CT=0.6 is ongoing.

Thermal environments. Hollows are less common at high latitudes, with none present at latitudes poleward of 78°N, suggesting solar heating plays an important role in hollow formation, consistent with previous findings [1–3]. The latitudinal range of hollows can help evaluate potential hollow-forming volatiles [8].

We find the smallest hollows are concentrated in relatively colder terrains (maximum temperatures <550 K at 1-m depth [9]), suggesting that warmer terrains provide more favorable growth conditions. Thermal mapping by BepiColombo will enable more detailed, localized studies of hollow thermal environments.

Topographic settings. The majority (77.5%) of hollows are located inside craters >20 km [10], suggesting cratering plays an important role in the excavation of hollow-forming volatiles. Work is ongoing to analyze how hollow class and size correlate with crater unit, size, and age as well as local slope and aspect to better understand hollow growth sequences.

Local host units. Previous studies found hollows are often located within low-reflectance blue plains and low-reflectance materials [11], suggesting the hollow-forming volatiles are prevalent in these units [1,2,5,8]. Interestingly, we find that most Class 2 hollows (at CT=0.8) are outside of these two units. Perhaps the local volatile supply is/was not as abundant, causing hollows to evolve to Class 2 more quickly.

Applications to BepiColombo: BepiColombo will collect visible-wavelength images of Mercury's surface for global mapping at <110 mpp [12]. We are ready to infuse the Mercury HORNET with BepiColombo data by applying transfer learning principles, allowing for immediate and optimized progress in hollow identification and change detections.

Acknowledgments: NASA Discovery Data Analysis Program, Grant #NNH21ZDA001N-DDAP.

References: [1] Blewett D. et al. (2011) *Sci, 333,* 1856. [2] Blewett D. et al. (2013) *JGRP, 118,* 1013. [3] Thomas R. et al. (2014) *Icar, 229,* 221. [4] Blewett D. et al. (2018), ed. by Solomon S. et al., *Cambridge U. Press,* 324. [5] Xiao Z. et al. (2013) *JGRP, 118,* 1752. [6] Speyerer E. et al. (2022) *GRL, 49,* 100782. [7] Bickel V. et al. (2020) *Nat Com, 11,* 2862. [8] Phillips M. et al. (2021) *Icar, 359,* 114306. [9] Siegler M. et al. (2013) *JGRP, 118,* 930. [10] Fassett C. et al. (2011) *GRL, 38,* 047294. [11] Klima R. et al. (2018) *GRL, 45,* 2945. [12] Da Deppo V. et al. (2010) *App Opt, 48,* 2910.